Development/Plasticity/Repair

GluN2B-Containing NMDA Receptors Promote Wiring of Adult-Born Neurons into Olfactory Bulb Circuits

Wolfgang Kelsch,* Zhijun Li,* Marina Eliava, Christina Goengrich, and Hannah Monyer
Department of Clinical Neurobiology, Medical Faculty Heidelberg and DKFZ, University Heidelberg, D-69120 Heidelberg, Germany

In the developing telencephalon, NMDA receptors (NMDARs) are composed of GluN1 and GluN2B subunits. These "young" NMDARs set a brake on synapse recruitment in neurons of the neonatal cortex. The functional role of GluN2B for synapse maturation of adult-born granule cells (GCs) in the olfactory bulb has not been established and may differ from that of differentiating neurons in immature brain circuits with sparse activity. We genetically targeted GCs by sparse retroviral delivery in mouse subventricular zone that allows functional analysis of single genetically modified cells in an otherwise intact environment. GluN2B-deficient GCs did not exhibit impairment with respect to the first developmental milestones such as synaptogenesis, dendrite formation, and maturation of inhibitory synaptic inputs. However, GluN2B deletion prevented maturation of glutamatergic synaptic input. This severe impairment in synaptic development was associated with a decreased response to novel odors and eventually led to the demise of adult-born GCs. The effect of GluN2B on GC survival is subunit specific, since it cannot be rescued by GluN2A, the subunit dominating mature NMDAR function. Our observations indicate that, GluN2B-containing NMDARs promote synapse activation in adult-born GCs that integrate in circuits with high and correlated synaptic activity. The function of GluN2B-containing NMDARs on synapse maturation can thus be bidirectional depending on the environment.

Introduction

New neurons are continuously added to the adult brain. The most abundant type of adult-born neurons are granule cell (GC) interneurons in the olfactory bulb (OB) (Lois and Alvarez-Buylla, 1993; Luskin, 1993). Adult-born GCs are generated in the subventricular zone (SVZ) and migrate to the OB where they form synaptic connections during a narrow time window (Carleton et al., 2003; Whitman and Greer, 2007; Kelsch et al., 2008). Only during this period of synaptic development, sensory deprivation changes the synaptic organization of glutamatergic synapses and increases cell death of adult-born GCs (Yamaguchi and Mori, 2005; Kelsch et al., 2009).

Sensory input-dependent development of glutamatergic synapses is regulated by NMDA receptors (NMDARs) in several types of neurons (Hensch, 2004). NMDARs are hetero-oligomers that contain the obligatory GluN1 subunit and variable GluN2 subunits. Upon deletion of GluN1 (ΔGluN1), the majority of adult-born GCs complete migration (Platel et al., 2010), but eventually die during synaptic development (Lin et al., 2010). Similarly, ΔGluN1 neurons in the adult dentate gyrus die during differentiation (Tashiro et al., 2006). While these studies clearly highlight the role for NMDAR-dependent survival of adult-born neurons, the function of NMDARs for synaptic development has remained unknown.

One wonders whether adult-born GCs undergo the same NMDAR-dependent synaptic development in a mature circuit as embryonically generated neurons given the different environments that the neurons encounter. Specifically, embryonically generated neurons face an environment with sparse synaptic activity. It was shown that under these circumstances GluN2B-containing NMDARs negatively regulate the incorporation of synaptic AMPA receptors (AMPARs) (Hall et al., 2007; Adesnik et al., 2008; Gray et al., 2011). In contrast to cortical development, adult-born neurons integrate into networks characterized by strong and concerted synaptic activity. In support of this hypothesis, reduction of the excitatory drive by systemic pharmacological inhibition of NMDARs can alleviate the increased cell death due to GluN1 deletion in adult-born neurons (Tashiro et al., 2006). Hence we set out to investigate NMDAR function for synapse maturation in adult-born neurons.

We targeted GluN2B by taking recourse to retroviral single-cell ablation of GluN2B (ΔGluN2B) in newly generated neurons assuming that adult-born GCs, like most neurons in the developing brain, are subject to the same maturational program with respect to their NMDAR subunit expression: initial GluN2B expression is followed by addition of GluN2A (Monyer et al., 1994; Hall et al., 2007; Adesnik et al., 2008; Gray et al., 2011). Sparse

Received March 26, 2012; revised May 5, 2012; accepted June 4, 2012.

Author contributions: W.K., Z.L., M.E., and H.M. designed research; W.K., Z.L., M.E., and C.G. performed research; W.K., Z.L., M.E., C.G., and H.M. contributed unpublished reagents/analytic tools; W.K., Z.L., M.E., C.G., and H.M. analyzed data; W.K. and H.M. wrote the paper.

The work was supported by a grant from the Schilling Foundation to H.M. and DFG grant KE1661/1-1 and a Fellowship of the Medical Faculty Heidelberg to W.K. We thank Dr. Anne Herb and Dr. Carlos Lois for continuous support and discussions; Dr. Georg Köhr for providing Grin2A-mutant mice; and Ulla Amtmann, Regina Hinz-Herkommer, and Preugschat-Gumprecht for technical help.

*W.K. and Z.L. contributed equally to this work.

The authors declare no competing financial interests.

Correspondence should be addressed to Dr. Hannah Monyer, Department of Clinical Neurobiology, Medical Faculty Heidelberg and DKFZ, University Heidelberg, Im Neuenheimer Feld 280, D-69120 Heidelberg, Germany. E-mail: h.monyer@dkfz.de.

Z. Li's present address: Department of Neurology, Tongji Medical College, Huazhong University, Wuhan 430010, China.

DOI:10.1523/JNEUROSCI.1459-12.2012

 0270-6474/12/3212603-09$15.00/0

dual retroviral labeling allows direct comparison of matched birth-dated neighboring adult-born GCs^{wt} and GCs$^{\Delta GluN2B}$, and circumvents indirect effects that might result from altered network activity, as often is the case in mice with gene deletions that affect larger brain areas. We observed that developmental NMDARs can function bidirectionally: in contrast to the previously described inhibitory action of NMDARs on synapse development in neonatal cortex, NMDARs in adult-born neurons promote synapse maturation and are thus required to develop functional glutamatergic synapses.

Materials and Methods

Retroviral vectors and mouse lines. Retroviral vectors were derived from a Moloney oncoretrovirus with an internal promoter fragment of the Rous sarcoma virus (MolR). Retroviral particles were produced and stored as previously described (Lois et al., 2002). The viral titers were $\sim 10^6$ infectious U/μl. Viral constructs were generated as follows: the stop codon of the genes of interest (palmitoylated *eGFP, SynaptophysinGFP, PSD-95GFP, GFPGluN2A,* and *GFPGluN2B*) was eliminated by PCR, and linked by a foot-and-mouth disease virus 2A sequence to the cDNA of Cre. Generation of MolR:(palmitoylated)GFP:2a:Cre and MolR:(NLS)mCherry was previously described (Lin et al., 2010). Retroviral constructs MolR:GFPGluN2A:2a:Cre and MolR:GFPGluN2B:2a:Cre were derived from previously published fusion proteins of NMDARs (von Engelhardt et al., 2009). Formation of functional channels by coexpression of GluN1 plasmids and MolR:GFPGluN2A:2a:Cre or MolR:GFPGluN2B:2a:Cre in HEK293 cells and recordings of NMDA-evoked currents (data not shown) confirmed that viral constructs delivered functional NMDAR subunits. pAAV-double floxed mCherry was a kind gift from K. Deisseroth and AAV was produced as previously described (Monory et al., 2006). Conditional knock-out (KO) mice for *Grin2B* (GluN2B$_{fl/fl}$) (von Engelhardt et al., 2008) and *Grin1* (GluN1$_{fl/fl}$) (Niewoehner et al., 2007), heterozygous lacZ reporter (B6-gt(ROSA) 26SOR lacZ) mice (Soriano, 1999), and *Grin2A* (GluN2A$^{-/-}$) KO mice (Sakimura et al., 1995) were bred in a C57BL/6N background (Charles River). Mice of either sex were used.

Stereotactic injections and mouse holding. All animal procedures were approved by the local Animal Welfare Committee. Retroviral injections were performed as recently described (Kelsch et al., 2008). All stereotaxic injections targeted the anterior SVZ (coordinates: anterior 1 mm; $\pm$0.9 mm lateral; ventral 2.1 mm in reference to bregma) of 2- to 5-month-old mice. All mice were kept in a 12 h daylight cycle under the same housing conditions.

Animal perfusion, histological processing, and immunohistochemistry. Mice were given an overdose of isoflurane and perfused transcardially with PBS at 37°C; subsequently they were perfused with 3% paraformaldehyde (PFA) and postfixed in 3% PFA for 12 h at 4°C. Fifty micrometer thick coronal slices were cut with a Leica vibratome. For quantification of genetic synaptic markers, sections were incubated in primary rabbit anti-green fluorescent protein (GFP) (1:4.000; Millipore Bioscience Research Reagents) antibody at 4°C overnight, and Alexa 555 secondary antibodies (1:750; Invitrogen) diluted in blocking solution for 2 h at room temperature. Blocking solution contained 0.25% Triton X and 1% bovine serum albumin. Sections were mounted with Fluoromount (Sigma). To visualize *c-Fos* expression a polyclonal rabbit antibody (1:10,000; Calbiochem) was used.

Survival analysis and fixed-ratio mix of two retroviruses. Two viruses were mixed at an approximate 1:1 ratio. For all time points and genotpyes in each experiment (see Fig. 1), the same batch of retrovirus mix was used. One of the viruses carried the construct encoding mCherry, while the other carried one of a range of constructs: Cre recombinase linked with the 2A linker to GFP, GFPGluN2A, and GFPGluN2B. The survival ratio is defined as the total number of GFP-positive cells (including double-labeled cells) divided by the number of singly labeled mCherry-expressing cells. Ten entire coronal sections per OB were analyzed using an Olympus epifluorescence microscope (20× objective). The survival ratio from each bulb was treated as one sample. These ratios of Cre$^+$ GCs$^{\Delta GluN2B}$ (including only GFP$^+$/Cre$^+$ GCs and both GFP$^+$/Cre$^+$ and mCherry$^+$ GCs) over only mCherry-expressing GCs^{wt} were determined in parallel in *wt* and GluN2B$_{fl/fl}$ mice (four mice per time point and genotype). For each time point, the mean ratio determined in GluN2B$_{fl/fl}$ mice was divided by the mean ratio established in *wt* mice, and the resulting normalized ratio expressed as "percentage of increased cell death" in GCs$^{\Delta GluN2B}$ relative to GCs^{wt} (1-normalized ratio, ×100). Statistical differences were determined between ratios of the two genotypes at the same time point (*t* test). SEM was calculated from pooled survival ratios of both genotypes. We performed several control experiments. We examined whether the age of the cell or the location within the rostral migratory stream (RMS) was critical for the survival of GluN2B-deleted new GCs at 7 d postinfection (d.p.i). The ratio of Cre$^+$/Cre$^-$ GCs was comparable in the RMS of the OB and genu of the RMS (0.89 $\pm$ 0.03, $n = 6119$ cells; 0.92 $\pm$ 0.12, $n = 3156$ cells, respectively; $p = 0.9$, *t* test) in three GluN2B$_{fl/fl}$ mice (n.s., *t* test).

Both GFP-tagged GluN2 subunits coexpressed with the obligatory GluN1 subunit formed functional channels *in vitro* (data not shown). LacZ reporter mice were used to compare the relative efficacy of Cre recombination among the different viral constructs (see Fig. 6). At 7 d.p.i., recombination had occurred in 92% GluN2B:GFP$^+$and 95% GluN2A:GFP$^+$ GCs as indicated by colabeling of GFP with β-gal ($n =$ 194 and 180 GCs, respectively, each in three lacZ reporter mice). We compared the efficacy of MolR:GFPGluN2A:2a:Cre (Fig. 6*C*) and MolR:GFP:2a:Cre (Fig. 1*B*) at 4 d.p.i.: recombination had occurred in 93% GluN2A:GFP$^+$ and 96% GFP$^+$ GCs as indicated by colabeling of GFP with β-gal ($n = 289$ and 326 GCs, respectively, each in three lacZ reporter mice; n.s., *t* test). These control experiments indicate that there was no difference in the efficacy of Cre recombination that might account for the differential effects in GC survival.

In utero injections into the lateral ventricles of E14 embryos were performed as previously described (Noctor et al., 2001) and analyzed in coronal cortical sections essentially as described for adult-born GCs in the OB.

Morphological analysis. Vibratome sections (150 μm) were incubated with rabbit polyclonal anti-GFP antibody (1:5000;Millipore) at 4°C for 24 h. Sections were sequentially incubated with biotinylated secondary antibody and with peroxidase-avidin-biotin complex (both biotinylated goat anti-rabbit and ABComplex from Vector Laboratories) and visualized with 3,3′-diaminobenzidine (DAB). Morphological reconstruction of the neurons and their processes was performed using the Neurolucida system (MBF Bioscience) with a 100× oil-immersion objective (Olympus microscope). Dendritic intersection numbers per 30 μm radius (Sholl analysis) and total length of dendritic trees were analyzed.

Genetic synaptic markers. Tissue processing and analysis of PSD-95GFP$^+$ clusters was performed as previously described (Kelsch et al., 2009). Confocal image stacks were acquired using a Zeiss LSM700 (63× oil-immersion objective) (512 × 512 pixel with pixel size of 0.196 × 0.196 μm), and with *z*-step 0.25 μm (80–150 sections). Maximal intensity projections were used to measure the density of PSD-95GFP$^+$ clusters of a dendritic segment with the integrated morphometry analysis of MetaMorph software (Universal Imaging). PSD-95GFP$^+$ clusters had to contain three or more adjacent pixels to be counted as a synaptic cluster. Expression of PSD-95GFP did not prevent death of GCs$^{\Delta GluN2B}$ as revealed by infection of GCs with a retrovirus mix (MolR:PSD-95GFP:2a:Cre and MolR:mCherry) in four GluN2B$_{fl/fl}$ and 4 *wt* mice. Adult-born GCs were examined at 28 d.p.i. The ratio of Cre$^+$/Cre$^-$ GCs was significantly decreased ($p < 0.001$, *t* test) in GluN2B$_{fl/fl}$ mice (0.03 $\pm$ 0.01) compared with *wt* mice (0.47 $\pm$ 0.04). PSD-95GFP$^+$ clusters are contacted by the presynaptic protein Bassoon in GCs (Kelsch et al., 2008) and PSD-95GFP was clustered at asymmetric synapses on an ultrastructural level (Livneh et al., 2009). To attribute PSD-95GFP$^+$ clusters (green fluorescence) to a particular GC, dendritic morphology was visualized by immunofluorescence with red-labeled antibodies against the diffuse PSD-95GFP present in the cytosol that was otherwise barely detectable (Kelsch et al., 2008). There were 92.4% GCs ($n = 689$) infected with MolR:SynaptophysinGFP:2a:Cre that had recombined in three lacZ reporter mice at 7 d.p.i. as indicated by coexpression of GFP and β-gal.

Electron microscopy. Brain tissue of GC$^{\Delta GluN2B}$ infected with MolR:PSD-95GFP:2a:Cre was further processed for ultrastructural evaluation.

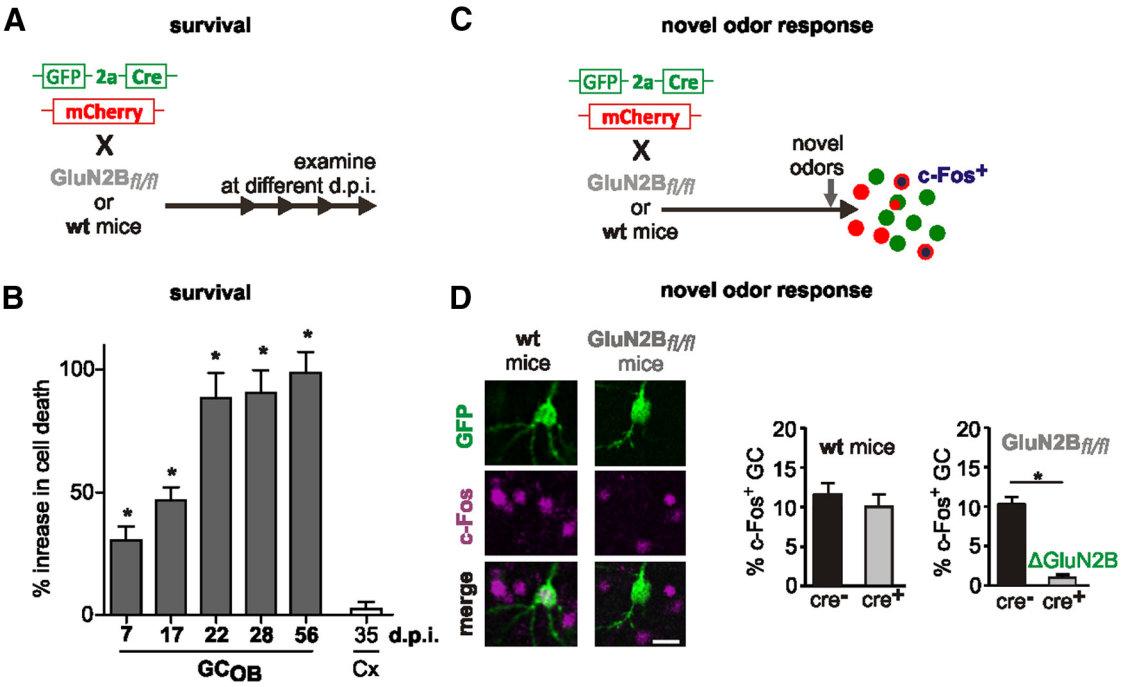

Figure 1. Differentiation of adult-born GCs $^{\Delta GluN2B}$ in the OB. ***A***, Survival of GCs $^{\Delta GluN2B}$ was determined at different d.p.i. with a fixed-ratio mix of two retroviruses in the SVZ of GluN2B$_{fl/fl}$ and *wt* mice. One virus controlled the coexpression of GFP and Cre-enzyme (MolR:GFP:2a:Cre), while the other virus, serving as a control (GCs ^{wt}), regulated nuclear mCherry expression (MolR:mCherry). ***B***, The ratio of Cre $^{+}$ GCs $^{\Delta GluN2B}$ (including only GFP $^{+}$/Cre $^{+}$ GCs and both GFP $^{+}$/Cre $^{+}$ and mCherry $^{+}$ GCs) over only mCherry-expressing GCs ^{wt} was determined in GluN2B$_{fl/fl}$ mice (4 mice per time point). The mean ratio determined in GluN2B$_{fl/fl}$ mice was divided by the mean ratio determined using the same retrovirus mix in *wt* mice for each time point and expressed as percentage increased cell death in GCs $^{\Delta GluN2B}$. As a control experiment neocortical neurons (Cx) were infected at E14 with the same retrovirus mix in GluN2B$_{fl/fl}$ and *wt* mice and examined 35 d later. Statistical differences were determined between ratios of the two genotypes at the same time point (*t* test). ***C***, Immediate-early gene expression (c-Fos) was assessed 1 h after exposure to novel odors in GCs at 17 d.p.i. with the retrovirus mix in GluN2B$_{fl/fl}$ and *wt* mice. ***D***, Representative confocal images of GFP and c-Fos coexpression in GCs in a *wt* mouse and lack of c-Fos expression in GFP $^{+}$ GCs in a GluN2B$_{fl/fl}$ mouse at 17 d.p.i. Scale bar, 10 μm. The percentage of c-Fos-expressing GCs $^{\Delta GluN2B}$ ($n = 396$) and GCs ^{wt} ($n = 254$) was examined at 17 d.p.i. in six GluN2B$_{fl/fl}$-mice ($p < 0.0001$). In parallel to GluN2B $^{fl/fl}$ mice, *c*-Fos expression of Cre $^{+}$ ($n = 402$) and Cre $^{-}$ GCs ($n = 170$) was examined in six *wt* mice upon odor exposure at 17 d.p.i. ($p = 0.46$). All data given as mean ± SEM, *t* test.

Tissue samples were taken from the GC layer and contained immunolabeled GC bodies and proximal parts of the apical dendrite. This portion of the GC is known to receive a high number of asymmetrical input synapses (Price and Powell, 1970). Four mice were transcardially perfused with the fixative containing 4% PFA and 0.1% glutaraldehyde. Free-floating 50 μm vibratome sections were incubated with rabbit polyclonal anti-GFP antibody (1:5000; Millipore) at 4°C for 24 h. Sections were sequentially incubated with biotinylated secondary antibody and with peroxidase-avidin-biotin complex (both biotinylated goat anti-rabbit and ABComplex from Vector Laboratories) and visualized with DAB. The DAB end product was enhanced using silver-gold intensification. The tissue was further processed for transmission electron microscopy (TEM). Briefly, the tissue was dehydrated in an ascending ethanol series and propylene oxide, immersed into Epon, flat-embedded, and polymerized between ACLAR sheets at 70°C. Areas of interest were cut out of the flat embedded tissue and re-embedded onto Epon blocks. Sixty nanometer thin serial sections were cut using a Leica Ultracut and placed onto pioloform-coated grids. Before analysis the grids were contrasted in aqueous solutions of uranyl acetate and lead citrate. The analysis was performed using a Zeiss LEO 910 TEM.

Bromodeoxyuridine labeling. Three- to five-month-old GluN2A $^{-/-}$ and matched *wt* mice received two intraperitoneal injections of 100 mg/kg body weight bromodeoxyuridine (BrdU) on the same day (12 h interval). BrdU sections were incubated in 1 M HCl before immunofluorescence staining with rat BrdU antibody (1:400; Accurate). Every sixth section was counted for each bulb. The total cell count of all sections was multiplied by six for each bulb and mean values for GluN2A $^{-/-}$ and matched *wt* mice were compared.

Novel odor stimulation. wt and GluN2B$_{fl/fl}$ mice were stereotactically injected with a retrovirus mix (MolR:GFP:2a:Cre and MolR:mCherry). At 17 d.p.i., IEG (c-Fos) response of GCs was assessed in mice that had no previous experience with the test odors (essentially following the procedure described by Magavi et al., 2005). Mice were housed individually in microisolator cages receiving 12 L/min of humidified, HEPA-filtered air for 24 h to reduce background activity. *wt* and GluN2B$_{fl/fl}$ mice were odor stimulated in parallel, and their brains were fixed, sectioned, and stained together to reduce variability. They were exposed to a set of odors for two intervals of 1 min separated by 1 min of exposure to clean air, to reduce potential effects of desensitization. Twelve liters per minute of HEPA-filtered humidified air was blown over filter paper moistened with the odor mix: imitation banana flavor, beef broth, chicken broth, yeast extract, imitation coconut vanilla extract, anise extract, almond extract, imitation rum, imitation orange, lemon extract, peppermint extract, imitation strawberry flavor, and olive oil. Immunofluorescence staining against GFP and c-Fos were examined in serial 50 μm sections using a Zeiss SPM5 confocal microscope (20× objective). All virally labeled cells in the GC layer were examined for coexpression of c-Fos. The percentage of c-Fos $^{+}$ expression in Cre $^{+}$ GCs (GFP-positive cells including double-labeled cells) and Cre $^{-}$ GCs (singly labeled mCherry-expressing cells) was determined.

Electrophysiology. Animals were given an overdose of isoflurane and perfused intracardially with cold (+4°C) slicing solution containing the following (in mM): 212 sucrose, 3 KCl, 1.25 NaH_2PO_4, 26 $NaHCO_3$, 7 $MgCl_2$, and 10 glucose (308 mOsm, pH 7.3). Bulbs were incubated in cold slicing solution and cut sagittally into 250 μm slices with a Mikrom vibratome. For recovery, slices were incubated at 32°C for 30 min in carbogenated recording solution containing the following (in mM): 125 NaCl, 2.5 KCl, 1.25 NaH_2PO_4, 26 NaHCO3, 1 $MgCl_2$, 2 $CaCl_2$, and 20 glucose (312 mOsm, pH 7.3). Fluorescence-guided, whole-cell patch-clamp recordings were performed with an EPC-10 amplifier (HEKA). For recordings of spontaneous postsynaptic currents (sPSCs), the pipette solution contained the following (in mM): 126 Cs-gluconate, 4 CsCl, 10 HEPES, 4 Mg-ATP, 0.3 GTP, 10 Tris-phosphocreatine, 2.5 QX-314-chloride, and pH 7.3. For recordings of evoked PSCs (ePSCs), the pipette

solution contained the following (in mM): 105 Cs-gluconate, 25 CsCl, 10 HEPES, 4 Mg-ATP, 0.3 GTP, 10 Tris-phosphocreatine, and 2.5 QX-314-chloride, pH 7.3. Successful patching onto the target cell was confirmed by identifying a fragment of fluorescent membrane trapped inside the pipette tip during or after the recording. Pipette resistance ranged from 7 to 9 MΩ, and cells were only accepted if pipette access resistance was <25 MΩ. The junction potential was not corrected throughout the study. For spontaneous EPSC (sEPSC) recording, synaptic events were collected at 32°C. Data were acquired with Patchmaster software (HEKA) and analyzed with IgorPro (Wavemetrics) software. All drugs were purchased from Tocris Bioscience.

Resting membrane potential was determined shortly after establishing the whole-cell configuration. Membrane capacitance and resistance were determined by application of a hyperpolarizing pulse. We recorded spontaneous instead of miniature PSCs, as in 2-week-old GCs the sPSC frequency is low and the block of action-potential-dependent release further decreases the frequency of events hampering statistical analysis at this stage of differentiation. Neurons were held at $V_m = -70$ mV (close to the reversal potential of 10 μM gabazine-sensitive sIPSCs) to record sEPSC. sPSCs recorded at $V_m = -70$ mV were blocked by 10 μM 6-cyano-7-nitroquinoxaline-2,3-dione (CNQX) at the end of the recording (data not shown). sIPSCs were recorded at $V_m = -40$ mV. sPSCs recorded at $V_m = -40$ mV were blocked by gabazine (10 μM). Ten minutes of continuous recordings was analyzed at the respective V_m. sPSCs were analyzed with Mini Analysis Program (Synaptosoft Inc.).

To record ePSCs, a unipolar glass stimulation electrode was positioned 30–50 μm from the soma in the GC layer. The stimulation intensity and position of the electrode was kept constant (20–50 μA) for the duration of the recording. In GCs$^{\Delta GluN2B}$ in which after blockade of evoked IPSC (eIPSC) by gabazine, no ePSCs could be evoked, the evoked EPSC (eEPSC) amplitude was considered zero for the excitation inhibition ratio. In cells expressing only eIPSCs, we increased the stimulation intensity up to 50-fold and repositioned the stimulation pipette along the dendrite, but could evoke no or only a small CNQX-sensitive eEPSC (data not shown). To determine AMPAR/NMDAR-mediated current ratio, amplitude, and kinetics, ePSCs were first evoked in control solution at $V_m = -70$ mV. Following blockade of eIPSCs by gabazine (10 μM), AMPAR-mediated eEPSCs were recorded that were subsequently blocked by 10 μM CNQX. Finally V_m was changed to +40 mV and NMDAR-mediated ePSCs were recorded and the 3 μM ifenprodil–sensitive component was determined. The remaining evoked currents at $V_m = +40$ mV were blocked by 50 μM D-AP5. Decay kinetics was determined from the average of 10 ePSCs with a double-exponential fit.

Statistical analysis. Except when otherwise indicated, data are reported as mean ± SEM and analyzed with the two-tailed Student's *t* test. A two-way ANOVA with Tukey's post test was used for Sholl analysis. Mann–Whitney test was used to compare the frequency of sPSCs, and ANOVA with Tukey's post test to test for drug effects on ePSCs.

Results

Survival and novel odor response of adult-born GCs$^{\Delta GluN2B}$

To determine whether adult-born GCs required GluN2B for survival, we infected GC precursors by injecting a fixed-ratio mix of two retroviruses into the SVZ of GluN2B$_{fl/fl}$ mice. One virus controlled the coexpression of GFP and Cre-enzyme (MolR:GFP:2a:Cre), while the other virus, serving to label control cells (GCs^{wt}), regulated nuclear mCherry expression (MolR:mCherry) (Fig. 1*A*). At 4 d.p.i. in the SVZ, recombination had occurred in 96.4% of Cre-expressing cells in the RMS of lacZ reporter mice as indicated by coexpression of GFP and β-gal ($n = 326$ cells in three mice). Ablation of GluN2B resulted in increased cell death of adult-born GCs. The majority of GCs$^{\Delta GluN2B}$ died between 17 and 22 d.p.i. (Fig. 1*B*). At earlier stages (7 d.p.i), there was a 30% reduction in GCs$^{\Delta GluN2B}$ survival in the OB, indicating that a subset of adult-born GCs requires NMDARs during migration. In contrast to adult-born GCs, survival of neocortical ΔGluN2B neurons was not affected when E14 precursors were infected with the same retrovirus mix and examined at P28 (Fig. 1*B*).

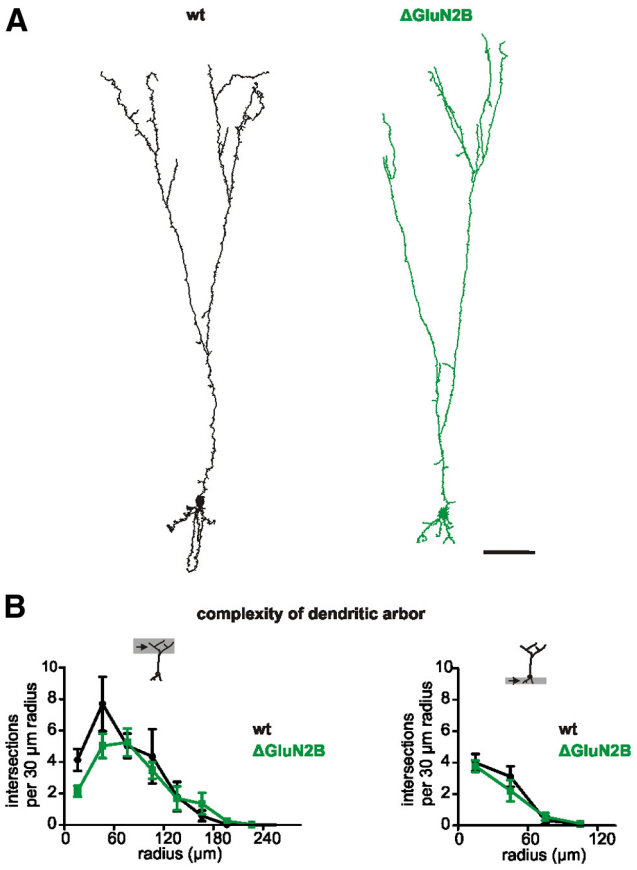

Figure 2. Dendritic morphology of GCs$^{\Delta GluN2B}$. ***A***, Reconstructions of adult-born GCs (17 d.p.i.) labeled with MolR:GFP:2a:cre in *wt* and GluN2B$_{fl/fl}$ mice. Scale bar, 50 μm. ***B***, The number of dendritic intersections per 30 μm radius is plotted against the radius from the starting point (9 reconstructed GCs$^{\Delta GluN2B}$ and 9 GCs^{wt} at 17 d.p.i with MolR:GFP:2a:Cre in 3 GluN2B$_{fl/fl}$ and 3 *wt* mice, respectively) (n.s., ANOVA). The starting point (0 μm) of basal dendrite equals the connecting point of the basal dendrite and the soma. The starting point (0 μm) of the distal apical dendritic domain equals the first branch point of the apical dendrite.

The remaining GCs$^{\Delta GluN2B}$ continued to die between 17 and 22 d.p.i., i.e., the time period when GCs exhibit enhanced responsiveness to novel odors as revealed by expression of the immediate early gene *c-Fos* (Magavi et al., 2005). Hence we injected the retrovirus mix into GluN2B$_{fl/fl}$ and *wt* mice and assessed immediate-early gene expression 1 h after exposure to novel odors in 17 d.p.i. GCs (Fig. 1*C*). We detected a significantly decreased number of *c-Fos*-expressing cells in the GCs$^{\Delta GluN2B}$ population compared with matched GCs^{wt} (Fig. 1*D*), suggesting impaired recruitment of GCs lacking GluN2B.

Dendritic differentiation and synaptic development of GCs$^{\Delta GluN2B}$

We therefore examined GluN2B-dependent cellular differentiation and synaptic development in new GCs. Morphological analysis at 17 d.p.i. revealed that GCs$^{\Delta GluN2B}$ had developed a normal dendritic tree with dendritic length (basal dendrite: 272 ± 27 vs 223 ± 27 μm, apical dendrite: 1330 ± 126 vs 1130 ± 127 μm; *t* tests n.s. for GCs^{wt}, $n = 9$ and GCs$^{\Delta GluN2B}$, $n = 9$, respectively) and complexity (i.e., number of dendritic intersections) comparable to that of GCs^{wt} (Fig. 2). At 17 d.p.i., GCs$^{\Delta GluN2B}$ protrusions along the dendrites were regularly detected (data not shown). Since filopodia and spines are difficult to distinguish in

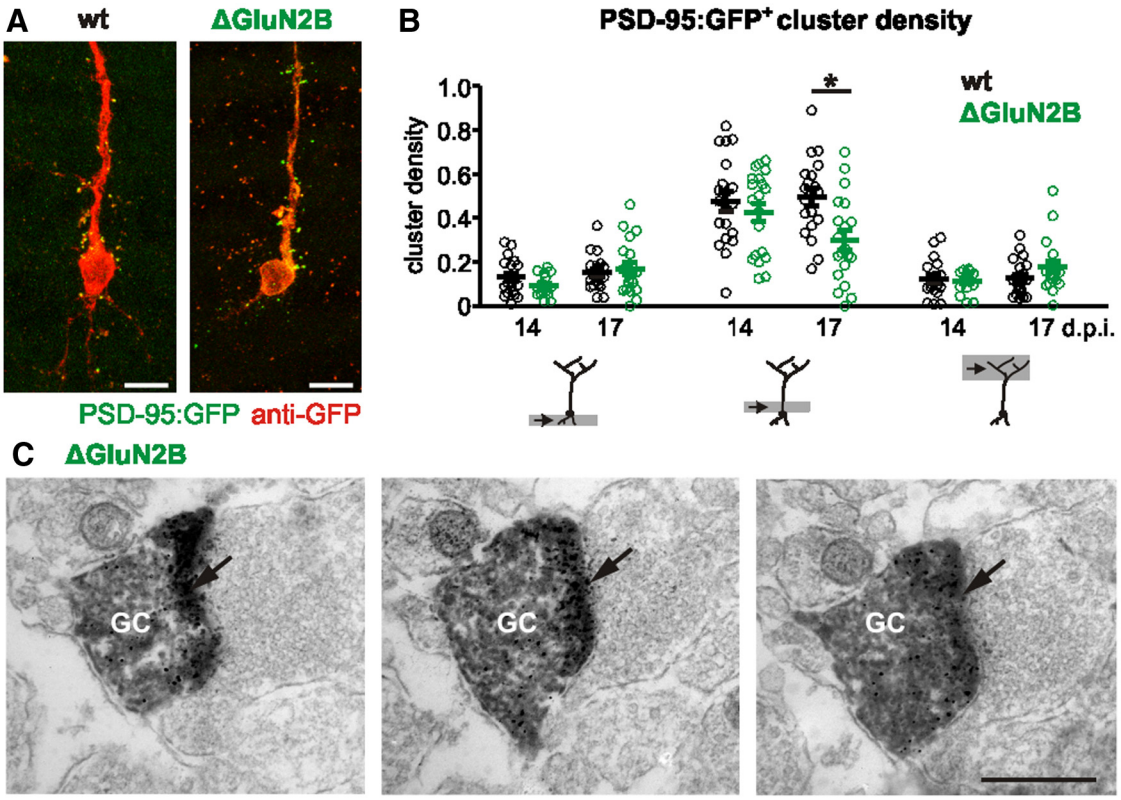

Figure 3. Synaptic development of GCs $^{\Delta GluN2B}$. ***A***, Densities of glutamatergic synapses were visualized using a genetic synaptic marker PSD-95GFP (MolR:PSD-95GFP:2a:Cre) in *wt* and GluN2B$_{fl/fl}$ mice at 17 d.p.i. Scale bar, 10 μm. To attribute PSD-95GFP $^{+}$ clusters (green) to a particular GC, dendritic morphology was visualized by immunofluorescence with Alexa 555-labeled antibodies (red) against the diffuse PSD-95GFP present in the cytosol that was otherwise undetectable. ***B***, Densities of PSD-95GFP $^{+}$ clusters were quantified in the three dendritic domains (basal, proximal, and distal domain (from left to right) of GCs $^{\Delta GluN2B}$ and GCs^{wt}, respectively, at 14 and 17 d.p.i. ($n = 20$ GCs in 4 *wt* and 4 GluN2B$_{fl/fl}$ mice for each time point). All data given as mean ± SEM, *t* test. ***C***, At 17 d.p.i., GCs $^{\Delta GluN2B}$ (MolR:PSD-95GFP:2a:Cre) were examined for the presence of asymmetric synapses. The images show three serial ultrathin sections of GC immunolabeled dendritic varicosity (GC) in GC layer of GluN2B$_{fl/fl}$ mice. The asymmetric postsynaptic density is visible on the dendritic site of the synaptic contact (arrow). The immuno-negative axon terminal contains round to spherical vesicles typical for asymmetric synapses. Scale bar, 600 nm.

immature neurons, we examined glutamatergic synapses using a retrovirus coexpressing the GFP-tagged synaptic marker PSD-95 and Cre recombinase (MolR:PSD-95GFP:2a:Cre) (Fig. 3*A*). Quantitative evaluation of synaptic densities indicated a differential loss of synapses along the dendritic tree in GCs $^{\Delta GluN2B}$ (Fig. 3*B*). While at 14 d.p.i. densities of PSD-95GFP $^{+}$ clusters in GCs $^{\Delta GluN2B}$ and controls were still comparable, by 17 d.p.i. there was a reduction of synaptic densities in GCs $^{\Delta GluN2B}$. The reduction was confined to the proximal dendrite, the compartment known to develop synaptic inputs first. As a presynaptic genetic marker we used SynaptophysinGFP (MolR:SynaptophysinGFP:2a:Cre). At 17 d.p.i., densities of SynaptophysinGFP $^{+}$ clusters in GCs $^{\Delta GluN2B}$ and GCs ^{wt} were comparable (0.13 ± 0.02 and 0.15 ± 0.01, $n = 20$, in four GluN2B$_{fl/fl}$ and four *wt* mice respectively; n.s., *t* test). Further evidence that glutamatergic synapses were formed on the proximal domain of 17 d.p.i. GCs $^{\Delta GluN2B}$ was obtained at the ultrastructural level ($n = 6$ synapses; Fig. 3*C*). Together, these findings suggest that dendritic differentiation and initial synaptogenesis occurred relatively independently of GluN2B-containing NMDARs for GCs that had survived NMDAR-dependent migration.

Functional maturation of glutamatergic synapses in GCs $^{\Delta GluN2B}$

We next examined functional properties of glutamatergic synapses in GCs $^{\Delta GluN2B}$ and matched GCs ^{wt} at 14–17 d.p.i. Passive membrane properties (resting membrane potential: −61.8 ± 0.7 vs −60.5 ± 0.8 mV, membrane resistance: 2.9 ± 0.4 vs 2.8 ± 0.4 GΩ, membrane capacitance: 5.9 ± 0.3 vs 5.6 ± 0.3 pF) were not significantly different for all three parameters in GCs ^{wt} and GCs $^{\Delta GluN2B}$ at 15–17 d.p.i. (22 and 24 cells, respectively, *t* test). To examine glutamatergic inputs to new GCs, we recorded 13 pairs of neighboring GCs $^{\Delta GluN2B}$ and GCs ^{wt} at 14–17 d.p.i. with the retrovirus mix (Fig. 4*A*). The average distance between GCs $^{\Delta GluN2B}$ and matched GCs ^{wt} was 65 ± 6 μm [range 50–100 μm]. The frequency of synaptic events in GCs of this age is low. We measured sEPSCs (recorded at $V_m = -70$ mV) and sIPSCs (recorded at $V_m = -40$ mV) in the same cell. sEPSCs were blocked by CNQX (10 μM; $n = 4$) and sIPSCs by gabazine (10 μM; $n = 4$, data not shown). While inhibitory synaptic inputs were regularly detected, the frequency and amplitude of spontaneous AMPAR-mediated glutamatergic inputs were significantly decreased in GCs $^{\Delta GluN2B}$ (Fig. 4*B–D*). These results suggest that GluN2B deletion in GCs impairs maturation of glutamatergic synapses.

To further explore the contribution of AMPAR- and NMDAR-mediated currents to EPSCs, we electrically evoked EPSCs in the perisomatic region. We examined perisomatic rather than distal glutamatergic inputs as they mature earlier and AMPAR- and NMDAR-mediated EPSCs were reliably evoked in all adult-born GCs ^{wt} at 15–17 d.p.i. (Fig. 5). Furthermore, proximal synapses already displayed a subtle impairment in the maintenance of synapse densities (Fig. 2) at this stage of differentiation. At this developmental stage, the NMDAR component was almost

completely blocked by the GluN2B inhibitor ifenprodil (3 μM) (Fig. 5*A–C*), whereas mature adult-born GCs^{wt} had only a small ifenprodil-sensitive NMDAR component (Fig. 5*A–C*) consistent with the developmentally regulated addition of ifenprodil-insensitive GluN2A-containing NMDARs. The ratio of AMPAR/NMDAR-mediated eEPSCs (recorded at $V_m = -70$ and +40 mV, respectively, with sequential block of the respective currents by CNXQ and D-AP5) remained in a comparable range in adult-born GCs^{wt} after 15–17 d.p.i. (2.1 ± 0.5 at 15–17 d.p.i, n = 7 cells; 2.2 ± 0.6 at 22–24 d.p.i, n = 7; 1.5 ± 0.2 at 42–44 d.p.i, n = 7) (ANOVA n.s.; same cells as in Fig. 5*A–C*). In contrast to matched adult-born GCs^{wt}, NMDAR-mediated eEPSCs could not be evoked in GCs$^{\Delta GluN2B}$ at 15–17 d.p.i. Furthermore, only small (10 μM) or no CNQX-sensitive AMPAR-mediated eEPSCs were detected (Fig. 5*D,E*), while gabazine-sensitive (10 μM) eIPSCs were reliably evoked at the same stimulation intensity and site in GCs$^{\Delta GluN2B}$ (Fig. 5*D,E*). Thus, following GluN2B deletion in adult-born GCs both NMDAR- and AMPAR-mediated EPSCs did not develop.

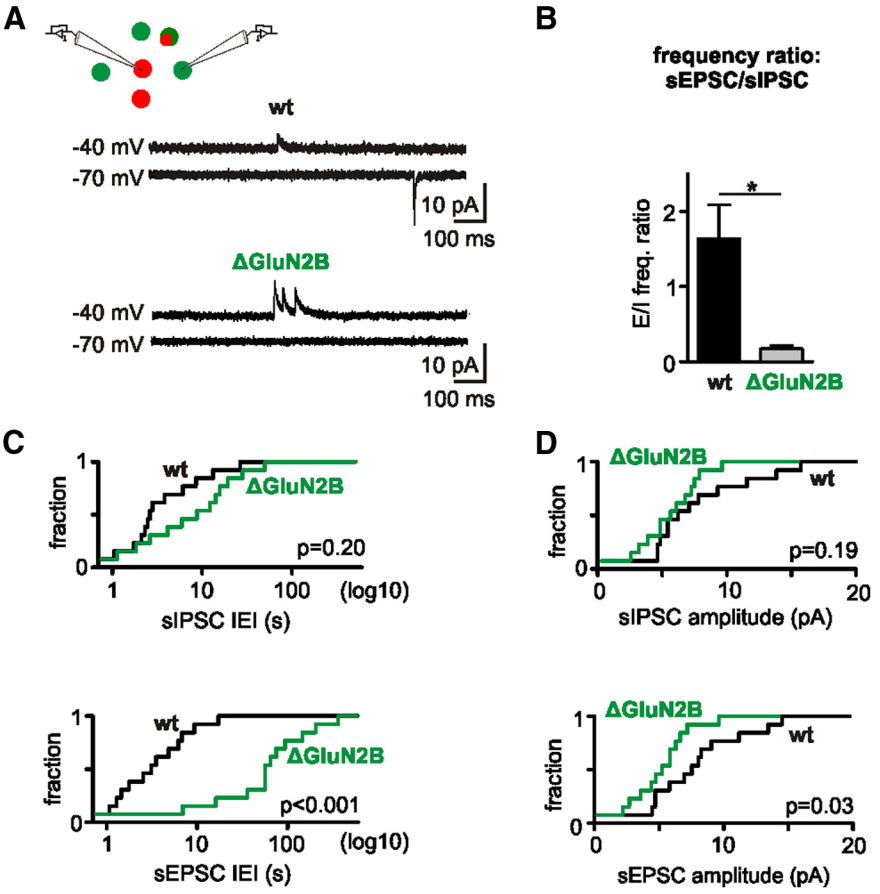

Figure 4. GluN2B-containing NMDARs are required to develop AMPAR-mediated sEPSC inputs. ***A***, sEPSCs and sIPSCs (V_m = −70 and −40 mV, respectively) were recorded in 13 pairs of neighboring GCs$^{\Delta GluN2B}$ and GC^{wt} at 14–17 d.p.i. with the retrovirus mix described in Figure 1. ***B***, Graph shows the ratio of sEPSC over sIPSC frequency for GCs$^{\Delta GluN2B}$ and neighboring GCs^{wt} (Mann–Whitney test). ***C***, Graphs show the cumulative distribution of IEI of sIPSCs and sEPSCs for GCs$^{\Delta GluN2B}$ and neighboring GCs^{wt} (Mann–Whitney test). The IEI was plotted logarithmically. ***D***, Graphs show the cumulative distribution of amplitudes of sIPSCs and sEPSCs for GCs$^{\Delta GluN2B}$ and neighboring GCs^{wt} (Mann–Whitney test).

Rescue of deletion of endogenous GluN2B by viral overexpression of GluN2 subunits

We subsequently addressed the question whether the integration of adult-born GCs into the OB circuit requires properties specific to GluN2B-containing receptors. We first tested the survival and development of adult-born GCs in mice lacking the GluN2A subunit. The quantification of labeled GCs at different time points following BrdU injection in GluN2A KO and *wt* mice indicated that GluN2A did not affect cell survival (BrdU$^+$ cells in GC layer per OB at 7 d.p.i.: 19,223 ± 1627 and 19,044 ± 1133, p = 0.93, t test; at 56 dpi: 12,567 ± 554 and 11,461 ± 696, p = 0.23, t test in five GluN2A$^{-/-}$ and five *wt* mice, respectively). Also the dendritic length of GCs in the two genotypes was comparable (apical dendrite: 1165 ± 75 and 1263 ± 86 μm, p = 0.39; basal dendrite: 244 ± 67 and 178 ± 38 μm, p = 0.4 for nine GCs in three *wt* and three GluN2A$^{-/-}$ mice, respectively). Dendritic complexity of GluN2A KO and *wt* mice did not differ (data not shown). GCs had comparable densities in glutamatergic input sites visualized by PSD-95GFP at 56 d.p.i. (basal domain: 0.51 ± 0.02 vs 0.52 ± 0.04, proximal ~: 0.69 ± 0.05 vs 0.56 ± 0.05, and distal ~: 0.45 ± 0.03 vs 0.44 ± 0.03, respectively, all t tests: n.s., n = 20 GCs from five GluN2A$^{-/-}$ and five *wt* mice, respectively). Finally, we performed rescue experiments and examined whether both GluN2B and GluN2A can restore the survival and development of adult-born GCs$^{\Delta GluN2B}$. Viral delivery ensured the expression of GFP-tagged GluN2A (MolR:GFPGluN2A:2a:Cre) or GluN2B (MolR:GFPGluN2B:2a:Cre) in GCs$^{\Delta GluN2B}$. These two viruses had a similar efficacy regarding Cre-mediated recombination as MolR:GFP:2a:Cre (see Materials and Methods). Infection of adult-born GCs with either of the two GFP-tagged GluN2 subunits resulted in formation of clusters along dendrites at 17 d.p.i. (tested in four GluN2B$_{fl/fl}$ mice, respectively; Fig. 6*C,D*). Of note, the loss of GCs following depletion of endogenous GluN2B, could be overcome upon GluN2B (Fig. 6*A*), but not GluN2A overexpression (Fig. 6*B*), denoting subunit specificity of GluN2 in promoting cell survival. Overexpression of GluN2A prevented cell loss in GCs$^{\Delta GluN2B}$ at 7 d.p.i. (Fig. 6*B*), but not at later stages (17–28 d.p.i.). Dendritic morphology GluN2A-overexpressing GCs$^{\Delta GluN2B}$ (Fig. 6*E*) in terms of dendritic length (basal dendrite: 250 ± 75 vs 290 ± 41 μm and apical dendrite: 1100 ± 81 vs 1312 ± 156 μm; t tests n.s. for GCs^{wt}, n = 9 and GCs$^{\Delta GluN2B}$, n = 9, respectively) as well as dendritic complexity (data not shown) had developed normally at 17 d.p.i. Thus, in summary GluN2B, but not GluN2A, is critical for survival and functional integration of adult-born GCs into the OB.

Discussion

Based on GluN2B KO in single cells, we demonstrate in this study that GluN2B-containing NMDARs are essential for the maturation of glutamatergic synaptic input, response to novel odors, and survival of adult-born GCs. Interestingly, lack of GluN2B in adult-born GCs does not preclude many of the early developmental steps like dendrite formation or synaptogenesis. GluN2B-containing NMDARs are a prerequisite for stable integration into

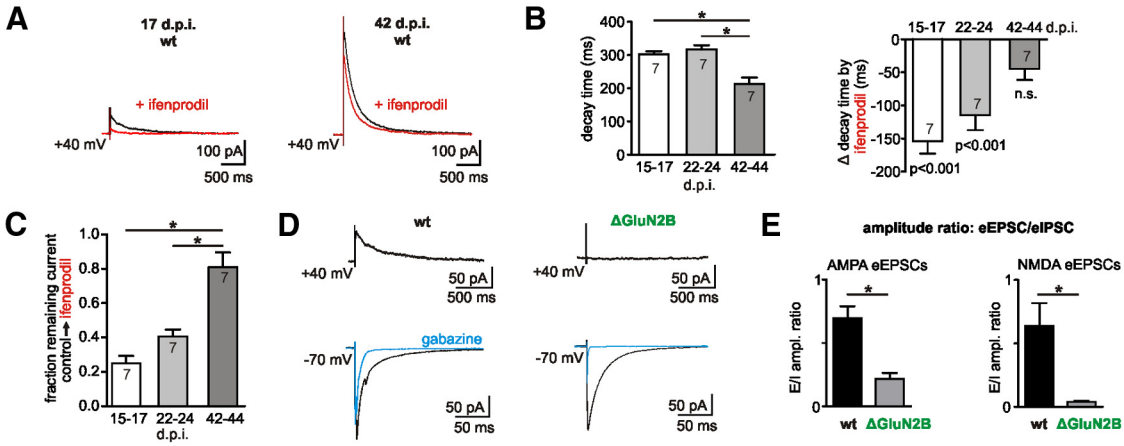

Figure 5. GluN2B-containing NMDARs are required to mature AMPAR-mediated glutamatergic synapses. ***A***, The GluN2B-antagonist, ifenprodil-sensitive (3 μM) NMDAR-mediated eEPSC component was determined in adult-born GCs in *wt* mice at 17 and 42 d.p.i with MoIR:GFP:2a:Cre. ***B***, Left, The decay kinetics of NMDAR-mediated eEPSCs became significantly faster during maturation of adult-born GCs (ANOVA $F_{(2,20)} = 13.7$, $p = 0.0002$; Tukey's post test: statistical significance is only indicated if $p < 0.05$). Right, The GluN2B-antagonist ifenprodil (3 μM) changed decay time of NMDAR-mediated eEPSCs more at earlier stages of GC maturation (*t* test). All data given as mean ± SEM. ***C***, The GluN2B-antagonist ifenprodil (3 μM) decreased the amplitude of NMDAR-mediated eEPSCs more at earlier stages of GC maturation (ANOVA $F_{(2,20)} = 23.1$, $p < 0.0001$; Tukey's post test: statistical significance is only indicated if $p < 0.05$). All data given as mean ± SEM. ***D***, Evoked gabazine-sensitive (10 μM) IPSCs were recorded in all GCs $^{\Delta GluN2B}$ and GCs ^{wt} ($n = 11$ and 10, respectively). D-AP5-sensitive (50 μM) NMDAR-mediated EPSCs (recorded at $V_m = +40$ mV) were only observed in GCs ^{wt} but not in GCs $^{\Delta GluN2B}$ (MoIR:GFP:2a:Cre in *wt* and GluN2B$_{fl/fl}$ mice). Whereas CNQX-sensitive (10 μM) AMPAR-mediated EPSCs (recorded at $V_m = -70$) were reliably evoked in GCs ^{wt}; no or only small AMPAR-mediated EPSCs were detected in GCs $^{\Delta GluN2B}$ at 15–17 d.p.i. The respective eEPSC components were blocked with D-AP5 and CNQX in all recorded cells to confirm their identity (data not shown). ***E***, Ratio of CNQX-sensitive (10 μM) AMPAR-mediated (left), or D-AP5-sensitive (50 μM) NMDAR-mediated (right) EPSC amplitude over gabazine-sensitive (10 μM) IPSC amplitude in 11 GCs $^{\Delta GluN2B}$ and 10 GCs ^{wt} at 15–17 d.p.i. All data given as mean ± SEM, *t* test.

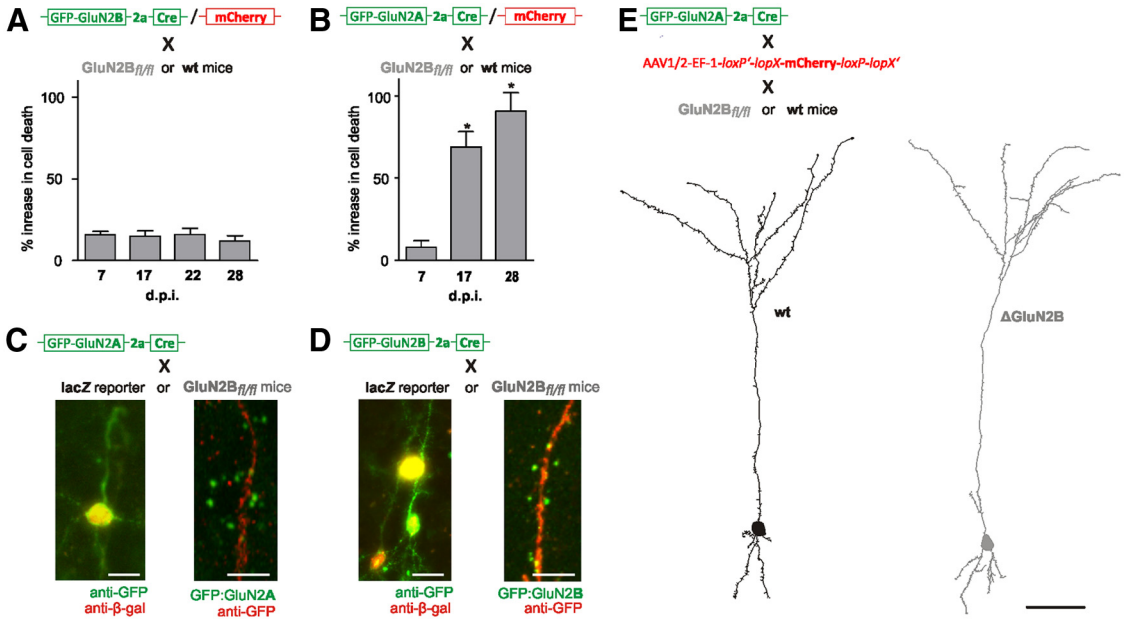

Figure 6. Overexpression of GluN2B, but not GluN2A, rescues survival in GC $^{\Delta GluN2B}$. ***A***, ***B***, A retrovirus mix (MoIR:GFPGluN2B:2a:Cre or MoIR:GFPGluN2A:2a:Cre and MoIR:mCherry) was injected to test for genetic rescue of GC survival by overexpression of GFP-tagged-GluN2B (***A***) and by GFP-tagged-GluN2A (***B***) upon depletion of endogenous GluN2B (4 *wt* and 4 GluN2B $^{fl/fl}$ mice for each d.p.i.) and analyzed as described in Figure 1 *B*. All data given as mean ± SEM, *t* test. ***C***, ***D***, Cre recombination efficacy of MoIR:GFPGluN2A:2a:Cre (***C***) and MoIR:GFPGluN2B:2a:Cre (***D***) was confirmed in three lacZ reporter mice, respectively. Scale bar, 10 μm. Both GluN2A- and GluN2B-overexpressing GCs formed GFP $^{+}$ clusters along the dendrites at 17 d.p.i. Scale bar, 5 μm. ***E***, To visualize the dendritic tree of GCs expressing the fusion protein of GluN2A, we coexpressed mCherry with AAV (pAAV-double floxed-mCherry) that only expresses mCherry upon recombination by retroviral Cre (from MoIR:GFPGluN2A:2a:Cre). Scale bar, 50 μm.

OB circuits since replacement by GluN2A cannot rescue the GluN2B KO phenotype.

Approximately one-third of adult-born GCs $^{\Delta GluN2B}$ died before differentiation in the OB begins. It is likely that this subpopulation coincides with the one described by Platel et al. (2010). These authors investigated the effect of GluN1 deletion in GCs, and found that the manipulation did not affect direction and speed of migration, but eventually resulted in the demise of a similar fraction of GCs in the RMS. The most likely cause for the 30% increase in early cell death reflects either an inhomogeneity in properties of GC precursors or variability in the timing of Cre-mediated recombination in the infected cell population. Based on our results, we conclude that both GluN2A and GluN2B provide trophic support for GCs during migration, indicating that survival signaling before synapse maturation is not NMDAR subunit specific. The lack of subunit specificity during migration

is in contrast with later developmental steps where GluN2B-specific functions cannot be substituted by GluN2A-containing NMDARs. The detailed characterization of the developmental profile is restricted to approximately two-thirds of GCs$^{\Delta GluN2B}$ that do not die during migration. Once GCs arrive in the OB, they exhibit a distinct developmental profile. Interestingly, certain milestones such as growth of the dendritic tree, initial formation of glutamatergic synapses, and development of GABAergic synaptic inputs do not require GluN2B-containing NMDARs. Normal acquisition of these neuronal properties in GCs$^{\Delta GluN2B}$ suggests that neurons that survived up to a certain point of differentiation were not generally impaired, but displayed relatively selective alterations in the maturation of glutamatergic synapses. NMDAR-independent dendrite formation is reminiscent of the development of cortical neurons born during embryogenesis (Ewald et al., 2008; Espinosa et al., 2009; Gray et al., 2011). Also the initial GluN2B-independent formation of glutamatergic synapses in adult-born GCs resembles the activity-independent synaptogenesis in embryonic development (Verhage et al., 2000). As maturation progresses, GluN2B deletion results in a loss of glutamatergic synapses that form first. Thus, adult-born GCs$^{\Delta GluN2B}$ that reach the OB undergo initially several steps of normal differentiation.

Thereafter, adult-born GCs develop functional synapses over a time period that begins 2 weeks after being born in the SVZ and ends by and large 2 weeks later (Carleton et al., 2003; Whitman and Greer, 2007; Kelsch et al., 2008). During this period of synaptic development, adult-born GCs expressed predominantly GluN2B-containing NMDARs that were blocked by the GluN2B-specific blocker ifenprodil. After completion of synaptic development, NMDAR-mediated EPSCs became largely insensitive to the GluN2B-specific blocker ifenprodil, reflecting the addition of GluN2A subunits that confer NMDARs mature properties.

The time period when GluN2B-containing NMDARs promote functional maturation of glutamatergic synapses of adult-born GCs coincides with the critical period of enhanced synaptic plasticity (Nissant et al., 2009). Only during this time period, sensory deprivation is associated with a change in synaptic organization and affects survival of adult-born GCs (Yamaguchi et al., 2005; Kelsch et al., 2009). GluN2B endows NMDARs with a low threshold for induction of activity-dependent synaptic modification (Kirkwood et al., 1996; Ge et al., 2007; Yashiro and Philpot, 2008), thereby promoting a transient period of developmental plasticity. The subsequent addition of GluN2A increases the threshold for activity-dependent modification of synapses (Kirkwood et al., 1996; Yashiro and Philpot, 2008) that concurs with the closure of the critical period when sensory input no longer affects synaptic organization and survival of the now mature adult-born GCs. Therefore dissecting the role of GluN2B is essential to understand the formation of stable synaptic contacts in the OB circuit. Upon GluN2B deletion, adult-born GCs initially developed glutamatergic synapses at normal levels, but soon thereafter the density of synapses decreased, suggesting that GluN2B-deficient synapses fail to be recruited and are eventually lost. The unique role GluN2B-containing NMDARs for synapse development in adult-born GCs is supported by our data showing that GluN2A-containing NMDARs did not rescue GC survival following GluN2B deletion. In contrast, adult-born GCs survived and developed normally in GluN2A$^{-/-}$ mice. In line with these results is a study reporting that replacing GluN2B with GluN2A globally in genetically modified mice was deleterious for the developing brain (Wang et al., 2011).

In conjunction with previous studies (Hall et al., 2007; Adesnik et al., 2008; Gray et al., 2011), our experimental data support the notion that GluN2B differentially affects synapse development in adult-born GCs and in neurons during cortical development: GluN2B deletion in adult-born GCs reduced the number of synapses, while the same manipulation in cortical neurons during perinatal development increased the number of active glutamatergic synapses. Thus, in stark contrast to the scenario reported here, GluN2B deletion in embryonically generated neurons led to an increase in the frequency of AMPAR-mediated EPSCs in the first postnatal weeks (P12—40), indicating that GluN2B-containing NMDARs negatively regulate the incorporation of synaptic AMPARs (Hall et al., 2007; Adesnik et al., 2008; Gray et al., 2011). Adult-born GCs, on the other hand, differentiate in mature circuits and require GluN2B-containing NMDARs to develop AMPAR-mediated EPSCs. Together, these studies prompt the hypothesis that the function of GluN2B-containing NMDARs is bidirectional depending on the environment: GluN2B-containing NMDARs promote synapse activation in adult-born GCs that integrate in circuits with high and correlated synaptic activity. In contrast, GluN2B-containing NMDARs exert a brake on synapse recruitment in the developing cortex. The opposing functions of NMDARs in the maturation of glutamatergic synapses in the developing and adult brain very likely account for the striking differences in NMDAR-dependent survival of differentiating neurons, whereas GluN2B-deficient neurons in the developing cortex survive normally, newly generated GluN2B-deficient neurons in the adult brain die during differentiation.

References

Adesnik H, Li G, During MJ, Pleasure SJ, Nicoll RA (2008) NMDA receptors inhibit synapse unsilencing during brain development. Proc Natl Acad Sci U S A 105:5597–5602.

Carleton A, Petreanu LT, Lansford R, Alvarez-Buylla A, Lledo PM (2003) Becoming a new neuron in the adult olfactory bulb. Nat Neurosci 6:507–518.

Espinosa JS, Wheeler DG, Tsien RW, Luo L (2009) Uncoupling dendrite growth and patterning: single-cell knockout analysis of NMDA receptor 2B. Neuron 62:205–217.

Ewald RC, Van Keuren-Jensen KR, Aizenman CD, Cline HT (2008) Roles of NR2A and NR2B in the development of dendritic arbor morphology *in vivo*. J Neurosci 28:850–861.

Ge S, Yang CH, Hsu KS, Ming GL, Song H (2007) A critical period for enhanced synaptic plasticity in newly generated neurons of the adult brain. Neuron 54:559–566.

Gray JA, Shi Y, Usui H, During MJ, Sakimura K, Nicoll RA (2011) Distinct modes of AMPA receptor suppression at developing synapses by GluN2A and GluN2B: single-cell NMDA receptor subunit deletion in vivo. Neuron 71:1085–1101.

Hall BJ, Ripley B, Ghosh A (2007) NR2B signaling regulates the development of synaptic AMPA receptor current. J Neurosci 27:13446–13456.

Hensch TK (2004) Critical period regulation. Annu Rev Neurosci 27:549–579.

Kelsch W, Lin CW, Lois C (2008) Sequential development of synapses in dendritic domains during adult neurogenesis. Proc Natl Acad Sci U S A 105:16803–16808.

Kelsch W, Lin CW, Mosley CP, Lois C (2009) A critical period for activity-dependent synaptic development during olfactory bulb adult neurogenesis. J Neurosci 29:11852–11858.

Kirkwood A, Rioult MC, Bear MF (1996) Experience-dependent modification of synaptic plasticity in visual cortex. Nature 381:526–528.

Lin CW, Sim S, Ainsworth A, Okada M, Kelsch W, Lois C (2010) Genetically increased cell-intrinsic excitability enhances neuronal integration into adult brain circuits. Neuron 65:32–39.

Livneh Y, Feinstein N, Klein M, Mizrahi A (2009) Sensory input enhances synaptogenesis of adult-born neurons. J Neurosci 29:86–97.

Lois C, Alvarez-Buylla A (1993) Proliferating subventricular zone cells in

the adult mammalian forebrain can differentiate into neurons and glia. Proc Natl Acad Sci U S A 90:2074–2077.

Lois C, Hong EJ, Pease S, Brown EJ, Baltimore D (2002) Germline transmission and tissue-specific expression of transgenes delivered by lentiviral vectors. Science 295:868–872.

Luskin MB (1993) Restricted proliferation and migration of postnatally generated neurons derived from the forebrain subventricular zone. Neuron 11:173–189.

Magavi SS, Mitchell BD, Szentirmai O, Carter BS, Macklis JD (2005) Adult-born and preexisting olfactory granule neurons undergo distinct experience-dependent modifications of their olfactory responses in vivo. J Neurosci 25:10729–10739.

Monory K, et al. (2006) The endocannabinoid system controls key epileptogenic circuits in the hippocampus. Neuron 51:455–466.

Monyer H, Burnashev N, Laurie DJ, Sakmann B, Seeburg PH (1994) Developmental and regional expression in the rat brain and functional properties of four NMDA receptors. Neuron 12:529–540.

Niewoehner B, Single FN, Hvalby Ø, Jensen V, Meyer zum Alten Borgloh S, Seeburg PH, Rawlins JN, Sprengel R, Bannerman DM (2007) Impaired spatial working memory but spared spatial reference memory following functional loss of NMDA receptors in the dentate gyrus. Eur J Neurosci 25:837–846.

Nissant A, Bardy C, Katagiri H, Murray K, Lledo PM (2009) Adult neurogenesis promotes synaptic plasticity in the olfactory bulb. Nat Neurosci 12:728–730.

Noctor SC, Flint AC, Weissman TA, Dammerman RS, Kriegstein AR (2001) Neurons derived from radial glial cells establish radial units in neocortex. Nature 409:714–720.

Platel JC, Dave KA, Gordon V, Lacar B, Rubio ME, Bordey A (2010) NMDA receptors activated by subventricular zone astrocytic glutamate are critical for neuroblast survival prior to entering a synaptic network. Neuron 65:859–872.

Price JL, Powell TP (1970) The synaptology of the granule cells of the olfactory bulb. J Cell Sci 7:125–155.

Sakimura K, Kutsuwada T, Ito I, Manabe T, Takayama C, Kushiya E, Yagi T, Aizawa S, Inoue Y, Sugiyama H (1995) Reduced hippocampal LTP and spatial learning in mice lacking NMDA receptor epsilon 1 subunit. Nature 373:151–155.

Soriano P (1999) Generalized lacZ expression with the ROSA26 Cre reporter strain. Nat Genet 21:70–71.

Tashiro A, Sandler VM, Toni N, Zhao C, Gage FH (2006) NMDA-receptor-mediated, cell-specific integration of new neurons in adult dentate gyrus. Nature 442:929–933.

Verhage M, Maia AS, Plomp JJ, Brussaard AB, Heeroma JH, Vermeer H, Toonen RF, Hammer RE, van den Berg TK, Missler M, Geuze HJ, Südhof TC (2000) Synaptic assembly of the brain in the absence of neurotransmitter secretion. Science 287:864–869.

von Engelhardt J, Doganci B, Jensen V, Hvalby Ø, Göngrich C, Taylor A, Barkus C, Sanderson DJ, Rawlins JN, Seeburg PH, Bannerman DM, Monyer H (2008) Contribution of hippocampal and extra-hippocampal NR2B-containing NMDA receptors to performance on spatial learning tasks. Neuron 60:846–860.

von Engelhardt J, Doganci B, Seeburg PH, Monyer H (2009) Synaptic NR2A- but not NR2B-containing NMDA receptors increase with blockade of ionotropic glutamate receptors. Front Mol Neurosci 2:19.

Wang CC, Held RG, Chang SC, Yang L, Delpire E, Ghosh A, Hall BJ (2011) A critical role for GluN2B-containing NMDA receptors in cortical development and function. Neuron 72:789–805.

Whitman MC, Greer CA (2007) Synaptic integration of adult-generated olfactory bulb granule cells: basal axodendritic centrifugal input precedes apical dendrodendritic local circuits. J Neurosci 27:9951–9961.

Yamaguchi M, Mori K (2005) Critical period for sensory experience-dependent survival of newly generated granule cells in the adult mouse olfactory bulb. Proc Natl Acad Sci U S A 102:9697–9702.

Yashiro K, Philpot BD (2008) Regulation of NMDA receptor subunit expression and its implications for LTD, LTP, and metaplasticity. Neuropharmacology 55:1081–1094.